Remote Sensing of Environment 162 (2015) 1–10

Contents lists available at ScienceDirect

Remote Sensing of Environment

journal homepage: www.elsevier.com/locate/rse

Land surface temperature retrieval over circumpolar Arctic using SSM/I–SSMIS and MODIS data

C. André [a], C. Ottlé [a,*], A. Royer [b], F. Maignan [a]

[a] Laboratoire des Sciences du Climat et de l'Environnement, Orme des Merisiers, 91191 Gif-sur-Yvette, France
[b] CARTEL, Université de Sherbrooke, Canada

ARTICLE INFO

Article history:
Received 3 August 2014
Received in revised form 23 January 2015
Accepted 24 January 2015
Available online 21 February 2015

Keywords:
Land surface temperature
SSM/I
SSMIS
Arctic
Permafrost
MODIS

ABSTRACT

Remote sensing instruments are key players to map land surface temperature (LST) at large temporal and spatial scales. In this paper, we present how we combine passive microwave and thermal infrared data to estimate LST during summer snow-free periods over northern high latitudes. The methodology is based on the SSM/I–SSMIS 37 GHz measurements at both vertical and horizontal polarizations on a 25 km × 25 km grid size. LST is retrieved from brightness temperatures introducing an empirical linear relationship between emissivities at both polarizations as described in Royer and Poirier (2010). This relationship is calibrated at pixel scale, using cloud-free independent LST data from MODIS instruments. The SSM/I–SSMIS and MODIS data are synchronized by fitting a diurnal cycle model built on skin temperature reanalysis provided by the European Centre for Medium-Range Weather Forecasts (ECMWF). The resulting temperature dataset is provided at 25 km scale and at an hourly time step during the ten-year analysis period (2000–2011). This new product was locally evaluated at five experimental sites of the EU-PAGE21 project against air temperature measurements and meteorological model reanalysis, and compared to the MODIS LST product at both local and circumpolar scale. The results giving a mean RMSE of the order of 2.2 K demonstrate the usefulness of the microwave product, which is unaffected by clouds as opposed to thermal infrared products and offers a better resolution compared to model reanalysis. The dataset can be downloaded from the PANGAEA website: http://doi.pangaea.de/10.1594/PANGAEA.833409.

1. Introduction

Land surface temperature (LST) variations are key parameters of northern climates, particularly as they are one of the most important factors determining the permafrost spatial distribution (e.g., AMAP-SWIPA report, 2011), the surface energy balance from the Earth's surface and the atmosphere (Hartmann et al., 2013), and terrestrial high-latitude ecosystem dynamics (Euskirchen et al., 2006; Kimball, McDonald, & Zhao, 2006; McGuire et al., 2007; Nemani et al., 2003; Running & Kimball, 2005). Fluctuations of ground temperature profiles are mainly governed by surface temperature temporal variations and the maximum depth of thaw reached every summer, the active layer thickness (Oelke, Zhang, Serreze, & Armstrong, 2003; Anisimov et al., 2007). Current observations show that northern climates are warming rapidly (Overland et al., 2014), which may have several effects on different ecosystems, hydrology, snow cover and climate, such as on active layer deepening in permafrost zones and soil freeze/thaw cycle (Goulden et al., 1998; Oelke, Zhang, & Serreze, 2004; Zhang, Chen, Smith, Riseborough, & Cihlar, 2005; Bunn, Goetz, Kimball, & Zhang, 2007; Anisimov et al., 2007), on soil–atmosphere gas exchange (Oechel et al., 1993; Matzner & Borken, 2008), and on plant phenology change over northern regions (Piao et al., 2008; Hashimoto et al., 2008; Kim, Kimball, Zhang, & McDonald, 2012).

The problem for the assessment of air or land surface temperatures and active layer variations over high latitudes in response to climate change is the very sparse distribution of meteorological stations and soil temperature measurements in high latitude areas (Anisimov et al., 2007; Kuzmina, Johannessen, Bengtsson, Aniskina, & Bobylev, 2008; Hinkel & Nelson, 2003; Lanckman, Elger, Karlsson, Johannsson, & Lantuit, 2013), added to this, is the large spatial heterogeneity of the surface temperature with the attendant problems of point measurements representativity. Satellite or reanalysis data with gridded spatial coverage can overcome this lack of ground-based observations.

Long time series of reanalysis data appear to be useful tools for climate analysis (Uppala et al., 2005; Bromwich, Fogt, Hodges, & Walsh, 2007; Mesinger et al., 2006). Air temperature output from the reanalysis dataset is relatively well calibrated and widely used (Betts, Ball, & Viterbo, 2003; Luo, Berbery, Mitchell, & Betts, 2007; Ma, Zhang, Li, Frauenfeld, & Qin, 2008; Tsuang, Chou, Zhang, & Roesch, 2008; Zou, Zhu, Zhou, Li, & Ma, 2014; Lindsay, Wensnahan, Schweiger, & Zhang, 2014). However, global reanalysis datasets are still provided at low spatial resolution, typically ERA-Interim data are on a grid cell of 0.75 × 0.75° (Dee, Uppala, Simmons, et al., 2011).

* Corresponding author.
E-mail address: catherine.ottle@lsce.ipsl.fr (C. Ottlé).

http://dx.doi.org/10.1016/j.rse.2015.01.028
0034-4257/

Remote sensing is known to be an adequate alternative to fill the gaps between stations, but with limitations depending on the approach used. Clouds and fog limit surface temperature derivation from thermal infrared sensors such as from MODIS or NOAA platforms. Therefore, thermal infrared sensor time series data must usually be composited over weekly, bi-weekly or even monthly periods (Gutman, Tarpley, Ignatov, & Olson, 1998; Sims et al., 2008), or otherwise an interpolation function must be applied to generate continuous time series over the year (Hachem, Allard, & Duguay, 2009). Moreover, as thermal LST data only correspond to cloud-free conditions, they are possibly biased for continuous temporal coverage and climate trend analysis, in particular over Arctic regions due to the abundance and frequency of clouds (Eastman & Warren, 2010; Westermann, Langer, & Boike, 2011). Recently, Catherinot et al. (2011) reviewed some methods to retrieve land surface temperature at global scale from microwave brightness temperatures. Some approaches are regional (Royer & Poirier, 2010), are somewhat dependent from ground-based point measurements (Holmes, De Jeu, Owe, & Dolman, 2009), but have been validated over specific areas (see Parinussa, de Jeu, Holmes, & Walker, 2008), other approaches are based on an iterative processes using physical parameters linked to specific land cover classes (Jones et al., 2010, 2007), or are relatively heavy to implement (such as the neural network inversion scheme developed by Aires, Prigent, Rossow, & Rothstein, 2001). Recently, Holmes, Crow, Tugrul Yilmaz, Jackson, & Basara, 2013 proposed a Kalman Filter-based assimilation scheme of multi-satellite microwave temperatures (Ka band observations) in a numerical weather prediction. They demonstrated the benefit of combining multiple microwave remote sensing-based and model-based temperature retrievals to enhance the accuracy of LST and to produce continuous time series.

Here we propose a new, simple empirical approach based on a pixel-by-pixel approach fitted to cloud-free satellite LST MODIS data, which accounts for the pixel-dependent variation of the microwave emissivity. The derived LST dataset is compared at local scale against LST MODIS data and analyzed over the circumpolar Northern Hemisphere (>45°N).

The datasets used are presented in the next section. In Section 3, we describe the methodology applied to retrieve the land surface temperature. Validation results of the generated northern circumpolar database are given and discussed in Section 4.

2. Datasets

Our area of interest is the northern high latitudes (>45°N) and our analysis period is from 2000 to 2011. The remote sensing data and the auxiliary datasets used to retrieve and validate the new land surface temperature series are presented in the following section.

2.1. Brightness temperatures from microwave satellite measurements

We used the vertically (v) and horizontally (h) polarized brightness temperatures at 37 GHz acquired by the Special Sensor Microwave Imager (SSM/I) and the Special Sensor Microwave Imager Sounder (SSMIS) passive microwave radiometric sensors, on board the Defense Meteorological Satellite Program (DMSP) polar-orbiting platforms (Armstrong & Brodzik, 1995) since 1987. Additionally and specifically for pixel masking purposes, we also used the vertically polarized brightness temperature at 19 GHz. We focus specifically on F13 (1995–2009) and F17 (2006–present) instruments. The dataset consists of temperatures projected on the Equal-Area Scalable Earth grid (EASE) for the Northern Hemisphere (Armstrong, Knowles, Brodzik, & Hardman, 1994). The spatial resolution is 25 km so that each image has a 721 × 721 pixel size and the satellite passes twice a day (ascending and descending) over most of the points. The ascending and descending equatorial crossing times for both F13 and F17 instruments are around 6:00 and 18:00 (local solar time) and the exact acquisition time for any pixel is in a time window about 2 h, depending on the point location. The same notation SSM/I will be used in the following to refer to the data of both instruments SSM/I and SSMIS.

2.2. Land surface temperatures from thermal infrared satellite measurements

We used LST from the Moderate Resolution Imaging Spectroradiometer (MODIS), operated by the National Aeronautics and Space Administration (NASA) within its Earth Observing System (EOS) program. MODIS sensors fly onboard the Terra (EOS AM, 2000–present) and Aqua (EOS PM, 2002–present) polar-orbiting platforms. MODIS LST, called in the following T_{MODIS}, was retrieved from thermal channel data (Wan, 2008), hence there are only clear-sky retrievals. LST data are available on a daily basis, with one day measurement and one night measurement, at global scale and at 1 km spatial resolution, along with the observation times. Both Terra and Aqua products were used, as their day and night observations are acquired at different times and these 2 instruments are well inter-calibrated on homogeneous and thermally constant targets (Xiong, Wu, & Cao, 2008). In both Aqua and Terra V5 products used, LST values at all grids are created from single clear-sky MODIS observations. As latitude increase beyond 30°, there may be multiple MODIS observations available due to overlapping swaths. Observations are then selected at smaller viewing zenith angles or at larger zenith angles if their values are greater at least 2 K. As a result, MODIS view time can form irregular temporal patterns. The summer 2007 T_{MODIS} products were used for calibration purposes and the summer 2008 products helped to evaluate the retrieved LST, called T_s in the following.

2.3. Reanalysis skin and air temperatures

We used skin temperatures obtained from the European Centre for Medium-Range Weather Forecasts (ECMWF) ERA Interim (ERA-I) reanalysis (Dee et al., 2011). We also use the ERA-I 2-meter air temperatures to validate the site measurements and the ERA-I precipitable water contents to estimate the atmospheric contribution. These data are available at a 0.75° × 0.75° spatial resolution with a 6-hour interval.

2.4. Local measurements

The evaluation was performed on five of the EU-PAGE21 field sites for which local air temperature measurements were available during our analysis period. Fig. 1 presents these sites and their location: Abisko

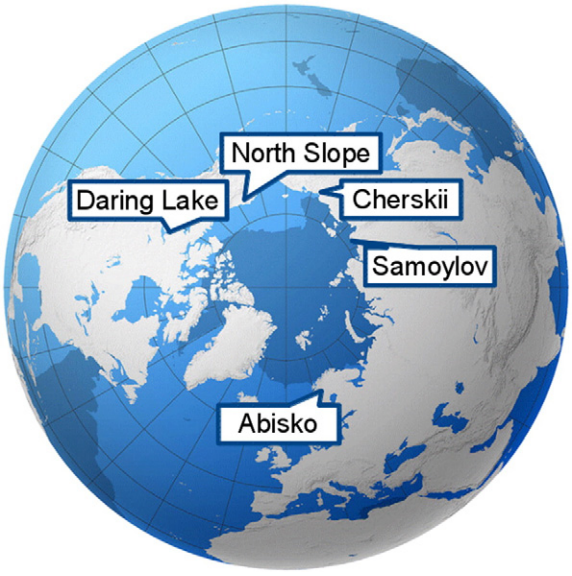

Fig. 1. Experimental sites used for the LST product validation. All these sites are part of the PAGE21 EU project.

(68.35 N, 18.82 E), Daring Lake (64.86 N, −111.56 E), Samoylov (72.37 N, 126.47 E), Cherskii (68.68 N, 161.53 E) and Betty Pingo station in North Slope (70.28 N, −148.89 E).

2.5. Land cover

The reliability of the retrieved LST depends on land cover. To evaluate the error for different land cover (LC) types at circumpolar scale, we used the European Space Agency (ESA) Climate Change Initiative LC map from the 2010 epoch (Bontemps et al., 2013, http://www.esa-landcover-cci.org). This global LC map was produced from various earth observation instruments including MERIS and SPOT-Vegetation under the ESA CCI. For specifically masking the ice cover and the continental shelf, we also use the EASE-Grid Land Cover Data Resampled from Boston University Version of Global 1 km Land Cover from MODIS 2001, Version 4 (Knowles, 2004).

3. Methodology

3.1. General background

The brightness temperature at the satellite level $T_p (p \in \{v, h\})$ is related to the land surface temperature (LST), T_s, by the following equation (assumed negligible the galactic contribution):

$$T_p = \tau\varepsilon_p T_s + \tau\left(1-\varepsilon_p\right)Ta_{\downarrow} + Ta_{\uparrow} \quad (1)$$

where ε_p is the surface emissivity for the polarization p, τ is the upward atmospheric transmission coefficient and $Ta_{\uparrow}$ and $Ta_{\downarrow}$ are the upward and downward atmospheric brightness temperatures respectively. The classical way to decorrelate LST and ε_p is to write this equation at two different polarizations and to assume a prior relationship between the two emissivities. At 37 GHz, Fily, Royer, Goïta, and Prigent (2003) found an empirical linear relationship between the surface emissivities over land, at vertical and horizontal polarizations:

$$\varepsilon_v = a\varepsilon_h + b \quad (2)$$

where $\varepsilon_{v/h}$ stands for surface emissivity at vertical and horizontal polarizations, and a,b are the linear regression coefficients. This closure relationship can be used to solve the radiative transfer equations at the same wavelength and for the two polarizations and to estimate LST, given knowledge of the atmospheric components and of the linear regression parameters a and b. Fily et al. (2003), followed later by Mialon, Royer, Fily, and Picard (2007),proposed, as a first approximation, to assume the atmospheric transmissivity and brightness temperatures to be constant and to use values of the a,b coefficients fitted on ground-based measurements, in order to estimate LST from 37 GHz SSM/I brightness temperatures, in snow-free conditions.

As already mentioned, the polar orbits of the SSM/I sensors provide global coverage of the Earth's surface twice daily. Therefore, if one wants to compare satellite-derived temperatures or to produce consistent time series, it is necessary to interpolate the measurements by taking into account the LST diurnal cycle. Thus, Mialon et al.(2007) and Royer and Poirier (2010) proposed to use the air temperature meteorological reanalysis, available at a 3 or 6-hourly time step, to produce hourly time series at pixel scale by interpolation with spline cubic functions. This methodology was developed and validated against air temperature measurements for North America on a daily basis with an absolute accuracy of about 3 K; the cumulative positive daily mean temperature was also used to compute a thawing index, which can be related to permafrost features (e.g., depth, top level temperature) and their trend in relation to climate warming (Mialon et al., 2007).

However, this approach fails when extended globally because the empirical coefficients and constant atmospheric assumptions are no longer valid and need to be revisited. Indeed, the atmospheric contributions in the radiative transfer equation are temporally and spatially dependent, and the relationship linking the polarized emissivities is strongly related to the landscape, especially to the sub-pixel open water and wetlands fractions and to the land coverage, in particular the forest cover (e.g., Pampaloni & Paloscia, 1985). Moreover, it appears that LST retrieval is very sensitive to uncertainties in the a,b coefficients (Eq. (2)) and thus particular attention should be paid to their estimation. Indeed, the impact of an error on the a,b coefficients for the LST retrieval process can be estimated by deriving LST with respect to a,b around the nominal point. The derivatives are given by Eqs. (3) and (4) and a first order of magnitude can be reached by prescribing the following values: $Ta_{\downarrow} = 31.8K$ (Fily et al., 2003), $b = 0.472$ (Royer & Poirier, 2010) and considering $\varepsilon_h = 0.85$ and $T_s = 273.15\ K$.

$$\frac{\partial T_s}{\partial a} = \varepsilon_h \frac{Ta_{\downarrow} - T_s}{b} \approx -435 \quad (3)$$

$$\frac{\partial T_s}{\partial b} = \frac{Ta_{\downarrow} - T_s}{b} \approx -511. \quad (4)$$

Since both a,b coefficients are around 0.5, a relative error of 1% on the latter induces an error of about 2.5 K on the retrieved LST. Given these features, we developed a new methodology for the inversion of the radiative transfer equation at pixel scale, taking advantage of the auxiliary measurements of the MODIS thermal infrared instruments, giving access also to LST in more limited clear-sky conditions.

3.2. New approach for separating LST and emissivity based on MODIS data

The new approach proposed to solve Eq. (1) is based on the assumption that the linear relationship linking the two polarized emissivities (Eq. (2)) is pixel dependent (spatially variable) and not temporally variable (i.e., the a,b parameters at 37 GHz can be assumed constant during the summer snow-free period). Thus, they can be estimated at the SSM/I pixel scale using the synchronous estimation of LST with MODIS data. Therefore, when combining Eq. (1) written for both polarizations with the closure Eq. (2), and assuming that the relationship linking polarized emissivities is still valid with (which means that the regression line passes close to the point $\varepsilon_h = \varepsilon_v = 1$), T_s can be written as follows:

$$T_s = k_1 \frac{T_v - Ta_{\uparrow}}{\tau} + k_2 \frac{T_v - T_h}{\tau} \quad (5)$$

where $k_1 = (1 - a)/b$ and $k_2 = a/b$.

Then, if coincident T_s estimates as well as atmospheric parameters are available, k_1 and k_2 parameters can be estimated for each pixel by least square regression over a given period. In the next section, we

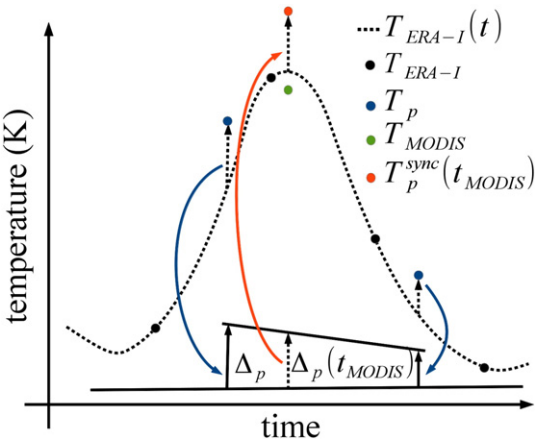

Fig. 2. T_p interpolation process based on the fit of the ERA-I temperature products to a diurnal cycle model.

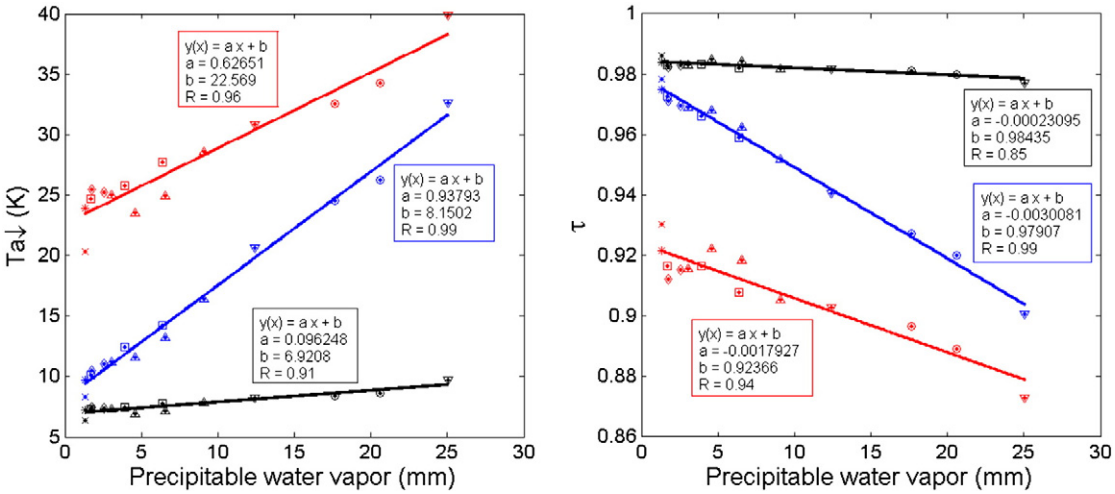

Fig. 3. Empirical relationships used to parameterize the atmospheric brightness temperature (left) and the atmospheric transmissivity (right), from precipitable water vapor. Red = 36.5 GHz, Blue = 18.7 GHz and Black = 10.7 GHz (from Roy, 2014).

present the algorithm that we developed to co-register and synchronize the MODIS and SSM/I data and estimate both k_1 and k_2 coefficients.

3.3. Algorithm presentation

In our algorithm, both k_1 and k_2 coefficients are estimated independently for the two satellites, F13 (1995–2009) and F17 (2006–present),during the training time overlap of summer 2007 to account for the intercalibration problem already highlighted by Cavalieri, Parkinson, DiGirolamo, and Ivanoff (2012).

Our methodology follows four consecutive steps. The first step consists of the application of a dedicated cloud mask on the MODIS data. Preliminary studies have shown that the MODIS cloud mask is not always reliable in the Arctic because of the low solar elevation and cold temperatures (Ackerman et al., 2008). These failures occur mostly during nighttime and lead to cold biases in the LST series (Østby et al., 2014; Westermann, Langer, & Boike, 2012). Therefore, it appears necessary to build a new mask to eliminate these cloudy pixels, since it is important to assess the surface temperature with the best possible accuracy. A filtering process is thus applied using a threshold based on the difference of the MODIS temperature with the skin temperature derived from meteorological reanalysis data. The threshold $th(\Delta_{MODIS}) = \mu(\Delta_{MODIS}) - \sigma(\Delta_{MODIS})$ is estimated independently for each pixel from the mean $\mu(\Delta_{MODIS})$ and the standard deviation $\sigma(\Delta_{MODIS})$ of the difference $\Delta_{MODIS} = T_{MODIS} - T_{ERA-I}(t_{MODIS})$ calculated for the summer calibration period, i.e., between DOY 170 and DOY 270 (mid-June to end of September). In the above equation, $T_{ERA-I}(t_{MODIS})$ is the ERA-I skin temperature interpolated at the time of the acquisition of MODIS by fitting a cubic spline.

The second step consists of co-registering the MODIS and SSM/I products spatially and temporally. The spatial co-registration is performed by projecting and averaging the MODIS datasets on the same EASE grid. The synchronization is achieved by fitting a diurnal cycle model as presented in Fig. 2, similar to what was proposed by Mialon et al. (2007); the difference being that we propose to use the ERA-I skin temperature product instead of the air temperature to model the LST diurnal cycle. Thus, we first calculate the differences $\Delta_P = T_p - T_{ERA-I}(t_{SSM/I})$, $p \in \{v, h\}$ between the SSM/I brightness temperatures

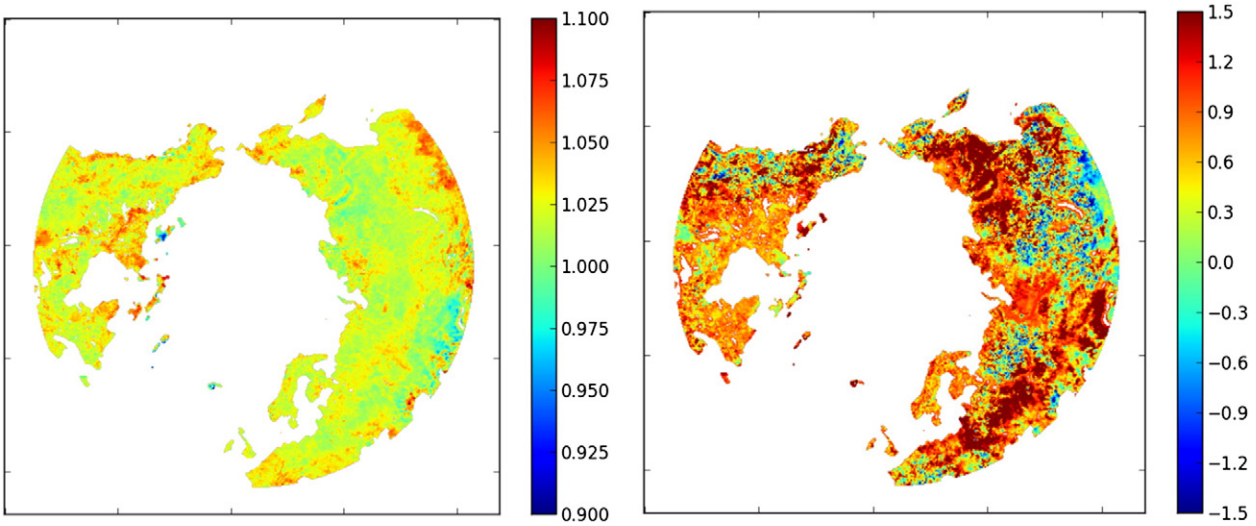

Fig. 4. Spatial variations of k_1 and k_2 parameters estimated for F17. Mean values are respectively 1.02 and 0.89.

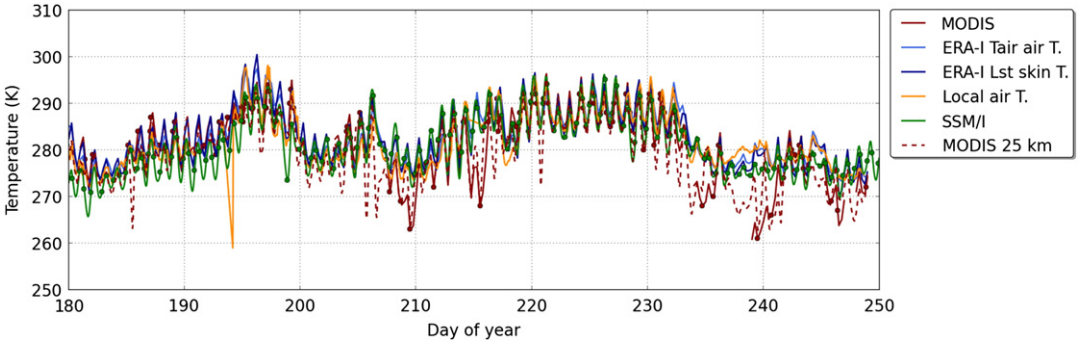

Fig. 5. Comparison of the SSM/I LST retrieval to MODIS product, ERA-I air and skin temperatures and local air temperature measurements at the Samoylov site over the snow-free period of 2008.

and the ERA-I skin temperature, similar to step 1. The Δ_P time series are then linearly interpolated and the differences $\Delta_P(t_{MODIS})$ are finally added to $T_{ERA-I}(t_{MODIS})$ to produce time series of SSM/I brightness temperatures interpolated at the time of the acquisition of MODIS that will be called $T_p^{sync}(t_{MODIS})$, $p \in \{v, h\}$ in the following.

Both k_1 and k_2 coefficients (Eq. (5)) are then calculated in the third step, on a pixel-by-pixel basis including the atmospheric correction. Over the calibration period, all available cloud-free T_{MODIS} were regressed against the corresponding $T_p^{sync}(t_{MODIS})$ corrected for the upward atmospheric transmission coefficient (τ) and the upward and downward atmospheric brightness temperatures assumed to be similar ($Ta_\uparrow \approx Ta_\downarrow$). The difference between the upward and downward atmospheric brightness temperatures are generally less than 1 K (Goïta & Royer, 2002; Kerr & Njoku, 1990; Roy, 2014). Both Ta and τ atmospheric parameters were derived from the empirical relationships given in Fig. 3 (Roy, 2014) as a function of precipitable water vapor derived from the Northern American Regional Reanalysis (NARR) data (Mesinger et al., 2006). The atmospheric parameters were modeled using the atmospheric "Millimeter-wave Propagation Model" (MPM: Liebe, 1989) implemented in the Helsinki University of Technology (HUT) snow emission model (Pulliainen, Grandell, & Hallikainen, 1999). The atmospheric model was driven with the air temperature and air moisture of the atmospheric layers above the surface from the 29 NARR atmospheric layers for different atmospheric environments (summer and winter arctic, subarctic and mid-latitudes). In the third processing step for retrieving LST from T_p, these relationships (Fig. 3) were applied using the precipitable water vapor derived from the global ERA-Interim reanalysis data.

The fourth step consists of snow, ice and ocean masking. To dynamically mask the snow covered pixels for which the T_s retrieval method is irrelevant, we used the spectral ratio $r = Tb_v(19\ \text{GHz})/Tb_v(37\ \text{GHz})$ between the vertically polarized brightness temperatures at 19 GHz and 37 GHz. The snow threshold $th_{snow}(r)$ is estimated from the mean $\mu_s(r)$ and the standard deviation $\sigma_s(r)$ of this ratio calculated over July and August 2007 by $th_{snow}(r) = \mu_s(r) + 3\sigma_s(r)$. The masking of the ice cover and of the continental shelf is also necessary because the assumption of linear dependence between ε_h and ε_v is irrelevant for ice covered areas and for mixed ground-sea pixels. Since the model is calibrated independently for each pixel, the mask can be applied either before or after the calibration process.

Finally, the (k_1, k_2) coefficients are estimated by least square regressions at the EASE grid scale, using all the data available during the calibration period of summer 2007. This calibration was performed independently for both F13 and F17 instruments to account for inter-calibration issues. There are indeed biases between the various SSM/I instruments which are well documented (see for example Royer & Poirier, 2010 for the previous DMSP satellites and Cavalieri et al., 2012 for F13 and F17). As an example, over the circumpolar Northern Hemisphere (latitudes >45°N), F13 and F17 brightness temperatures at 37 GHz present a root mean square difference around 3 K for both polarizations and a bias of 1 K over summer 2007. If the parameters of the retrieval process are estimated without considering these discrepancies, the retrieved LSTs will present the same biases. To solve this issue, we have calibrated separately our LST retrieval model on the same MODIS LST data over the same overlap period (summer 2007), and estimated a set of coefficients (k_1, k_2) for each instrument. Then, the Ts values can be retrieved for all snow-free pixels for the entire study period, i.e., 2000–2011, and interpolated at an hourly time step, using the same diurnal cycle model based on ERA-I skin temperatures, to produce continuous hourly time series.

Spatial variations of k_1 and k_2 estimated for F17 are shown in Fig. 4. The mean and standard variation values of k_1 are respectively 1.026 and 0.012. These values are fairly close to the ones obtained for F13, respectively equal to 1.029 and 0.011. However, this is not the case with k_2 for which the mean and standard variation values are respectively 0.89 and 0.74 for F17 and 0.68 and 0.52 for F13.

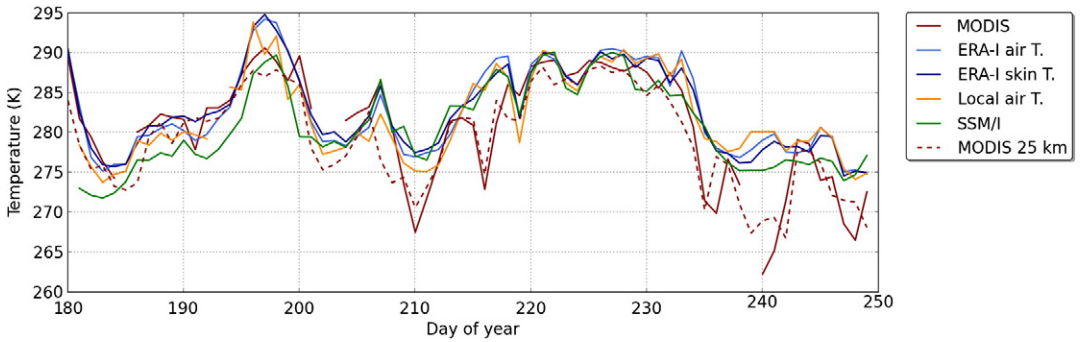

Fig. 6. Same as Fig. 5 but for daily mean temperatures (Samoylov site over 2008).

Table 1
Biases, RMSE and correlation coefficients between daily mean air temperatures measured on field against ERA-I, MODIS and SSM/I products (Samoylov site over 2008).

	ERA-I air T.	ERA-I skin T.	MODIS	MODIS (25 km)	SSM/I
Bias (K)	0.7	0.8	−1.9	−2.8	−0.38
RMSE (K)	1.7	2.0	5	4.5	2.6
Correlation	0.94	0.92	0.79	0.75	0.89

Table 2
Biases and RMSE of daily SSM/I-derived against MODIS temperature for all the field measurements considered (see Fig. 1) and over snow free period of 2008.

	Abisko	Samoylov	Daring Lake	North Slope	Cherskii	All
Bias (K)	−0.2	0.37	−0.24	−0.16	−0.26	−0.1
RMSE (K)	1.68	2.69	1.00	1.75	1.55	1.73

4. Results

4.1. Evaluation at local scale

The evaluation of our LST time series was performed at local scale on all the sites listed in Section 2.4, and during summer 2008 for which MODIS data were also processed, except for Cherskii for which field measurements are only available for 2009. Due to the high spatial heterogeneity of LST, the comparison between low resolution product and local field measurements is questionable and requires to apply upscaling methods accounting the spatial variability (see for example Westermann et al., 2011). The retrieved LST were therefore evaluated against MODIS LST which are more representative at the EASE grid scale. The in-situ (2 m) air temperature measurements and ERA-Interim re-analysis data are also given as they can be considered as a proxy estimate at kilometer scales (Hachem, Duguay, & Allard, 2012; Soliman, Duguay, Saunders, & Hachem, 2012), even if air temperature can show some discrepancies from LST depending on land cover and soil moisture state (Becker & Li, 1995; Kalma, McVicar, & McCabe, 2008 and Trigo, Monteiro, Olesen, & Kabsch, 2008).

Figure 5 presents the comparison obtained for the Samoylov site (Boike et al., 2013). The ERA-I skin temperature, ERA-I air temperature (2 m), MODIS observations, the SSM/I retrieved LST as well as the in-situ air temperature (2 m) are compared. MODIS and SSM/I observations were interpolated by fitting the ERA-I skin temperature. Moreover, two MODIS curves are plotted: the plain line interpolates 1-km MODIS LST observations for the site and the dashed line interpolates MODIS LST aggregated for the 25 × 25 km area covered by the SSM/I pixel. It should be noted that the aggregated LST is computed if at least 10% of the 25 × 25 pixels are cloud free. This explains that the 1-km MODIS curve (plain red) may present discontinuities linked to cloudiness whereas the 25-km MODIS curve (dashed red) remains continuous. To highlight the deficiencies of the cloud masking in the original product, the MODIS filtering process presented in Section 3.3 is not applied on the data shown on these plots.

By using both Aqua and Terra MODIS data, at least one measurement per day is obtained for 55 days over the 70-day period analyzed. Figs. 5 and 6 (showing the daily mean temperature variations) illustrate two points. First, cloud filtering errors on MODIS data occur mostly at night. Indeed, the bias between MODIS and air temperature field measurements is equal to −0.5 K for daytime and −3.1 K for nighttime, mainly due to some pronounced minimum peaks during the period. Second, MODIS passes over Samoylov around midday and midnight while F17 passes around 6 h 00 and 18 h 00. MODIS can thus better measure the diurnal cycle and the daily maximum than SSM/I. The diurnal cycle fitting model applied to the SSM/I observations can reproduce the diurnal amplitude of LST, but this amplitude seems to be slightly underestimated compared to MODIS estimates. This over-smoothing of the diurnal cycle could be the result of the coarse spatial resolution of the ERA-I product used (i.e., 0.75°) and/or a consequence of a bad representation of daily minimum and maximum temperatures by the spline cubic interpolation applied on 6-hourly meteorological data, as shown by Aires, Prigent, & Rossow, 2004.

Fig. 6 shows daily mean temperatures at Samoylov during the same period and biases, RMSE and correlation coefficients calculated between daily mean air temperatures measured on field against other products are shown in Table 1.

ERA-I air temperature is in good agreement with field measurements with a correlation coefficient of 0.94. This agreement was already highlighted by Langer et al. (2013) for the same site. The ERA-I skin temperatures are also strongly correlated to in-situ LST. The deviation of MODIS LST relative to field measurements is larger than both ERA-I air and skin temperatures, with a negative bias. However, these biases are also explained by the cloud filtering errors that could result in strongly underestimated temperatures (Langer, Westermann, & Boike, 2010). The clear sky requirement for MODIS observations also implies some wide gaps between consecutive data.

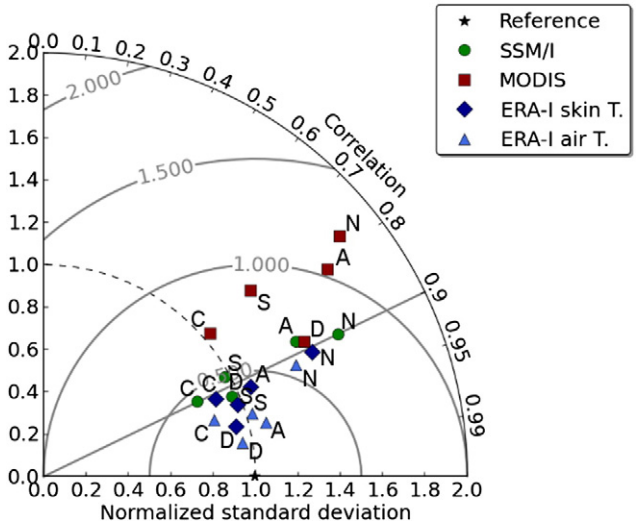

Fig. 7. Taylor diagram. The experimental sites are represented by the following letters: A: Abisko, C: Cherskii, D: Daring Lake, N: North Slope, S: Samoylov.

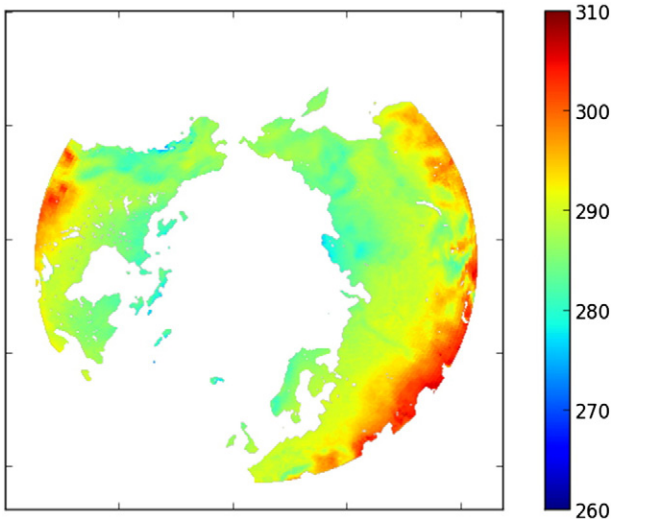

Fig. 8. Mean summer SSM/I-LST (DMSP-F17), for 2007 at circumpolar scale (temperatures are in Kelvin).

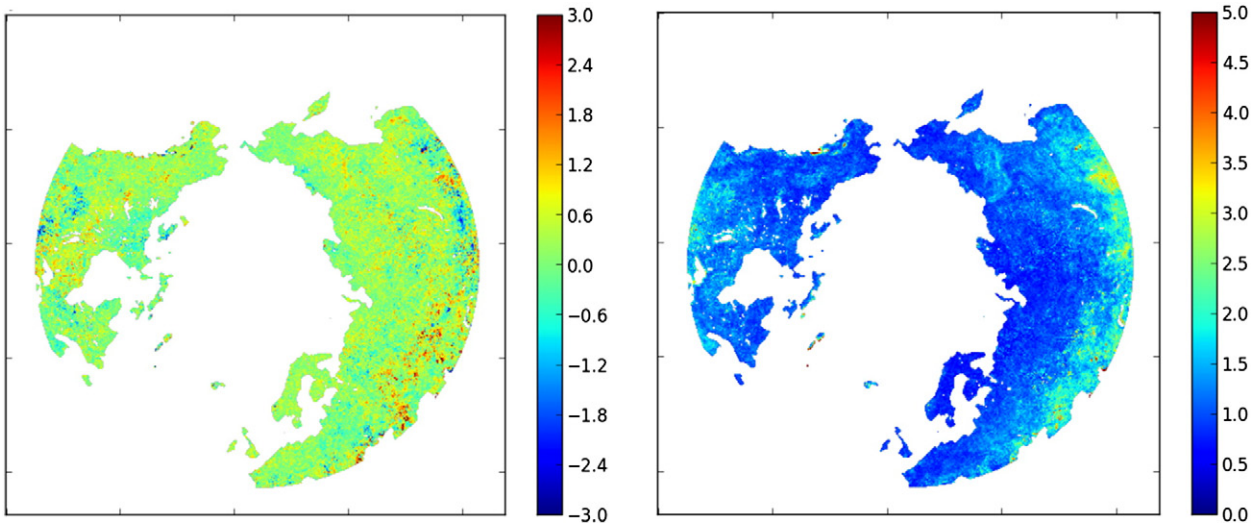

Fig. 9. Biases (left) and RMSEs (right) between LSTs retrieved from F13 and F17 brightness temperatures for summer 2008 (units are in Kelvins).

The SSM/I LST is in better agreement with air temperature field measurements (bias ≈ -0.38 K, RMSE ≈ 2.6 K) than with MODIS, however we can see that SSM/I systematically underestimate the temperature before the 200th day of year (bias ≈ -1.6 K). It can be noted that this early summer bias is observed each year in Samoylov in our dataset. One explanation could be the presence of ice on water bodies as reported by both Langer et al. (2010) and Westermann et al. (2011). The ice strongly affects the surface emissivity and the polarization ratio (Derksen et al., 2009); it could thus lead to a slight underestimation of the temperature retrieved. This observation may stress some weaknesses in the flagging of ice cover in our procedure, especially in the case of subpixel coverage.

The results obtained for all the experimental sites are summarized in Fig. 7. The Taylor diagram (Taylor, 2001), shows the correlation (cosine of azimuthal angle), normalized standard deviation (radial distance to the origin) and centered root mean square difference (distance to point x = 1 on the x-axis) for all sites against the air temperature local measurements, calculated for SSM/I, MODIS, ERA-I LST and ERA-I air temperature data series at daily time scale. The results clearly show the good correlation (around 0.9) obtained for all sites between our LST product derived from SSM/I data, the ERA-I products and the local measurements. The ERA-I air and skin temperatures are in better agreement with the in situ air temperatures and that was expected. However, our product offers a much better resolution (25 km compared to 0.75° for ERA). Fig. 7 shows the added value of the microwave LST product compared to the MODIS estimates, which appear noisier. The North Slope site has larger standard deviation (*std*) values whatever the product used compared to the local measurements (Fig. 7). This could be explained by the fact that this site is located near the Arctic Ocean (Fig. 1). Therefore the local meteorology could significantly differ from the large-scale meteorology derived from the ERA-I reanalysis considering that the pixel is considered as continental. The Abisko site also has a large *std* which could be the consequence of the larger noise observed in the MODIS data for that site, which seems to be more cloudy than the other ones. This observation error could have propagated in the inversion model and lead to a larger uncertainty on the SSM/I estimate.

Note that the diagram (Fig. 7) does not provide information about overall biases, but solely about the centered error. Biases and root mean square errors of daily SSM/I-derived against MODIS temperature

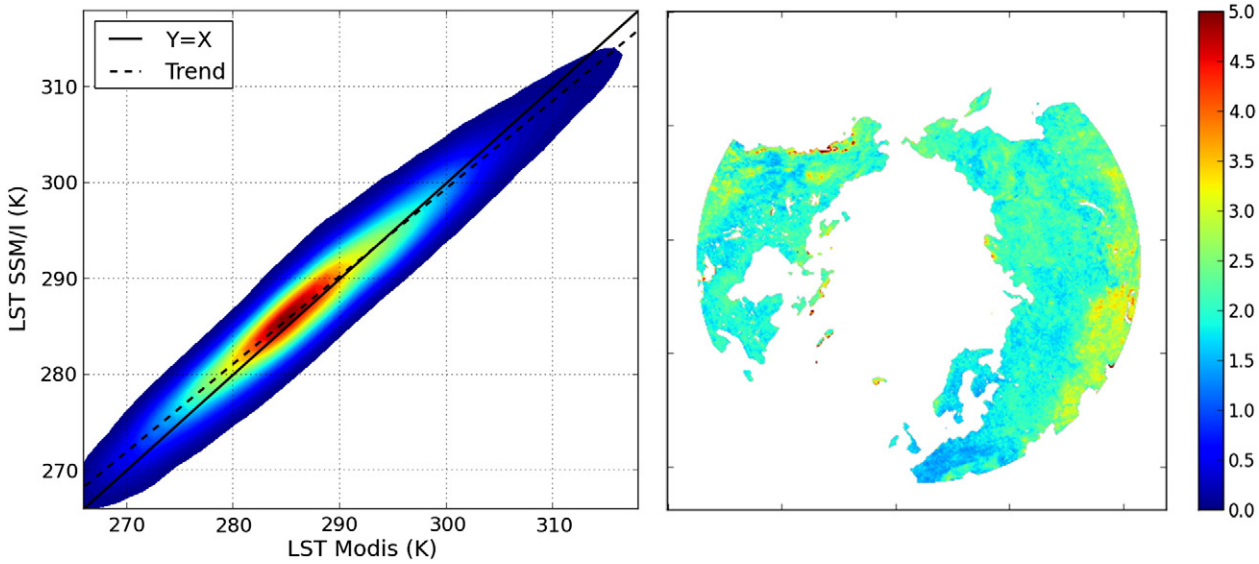

Fig. 10. Scatterplot between the SSM/I-derived temperatures and the MODIS LST (left) and the distribution of the RSMEs (right) for summer 2008. The colors in the scatterplot correspond to the density of points.

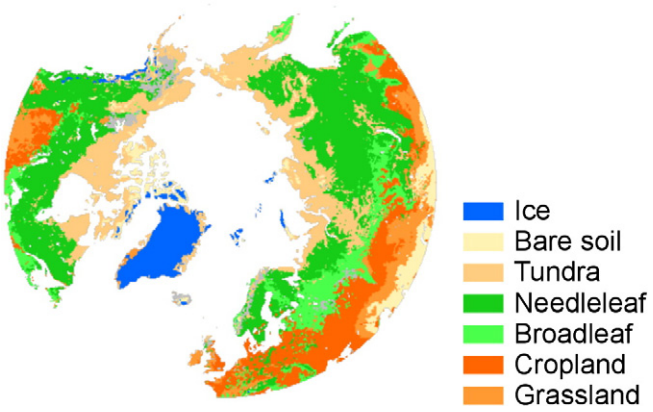

Fig. 11. ESA CCI land cover map (Bontemps et al., 2013). The ice covered areas were not considered in the analysis.

for all sites are shown in Table 2. For the 5 sites considered, the mean bias is −0.1 K and the mean RMSE is 1.73 K (Table 2).

The RMSE of the daily SSM/I-derived temperatures against the MODIS temperatures shown in Table 2 is larger for Samoylov compared to all the other sites. This could be explained by the larger fraction of free water (0.4) observed in Samoylov compared to the other sites (up to 0.2). The possible presence of remaining frozen water during early summer (as already mentioned above), could have increased the error in the temperature retrieval.

4.2. Evaluation at circumpolar scale

As an example, the mean summer LST at circumpolar scale obtained from F17 data for July and August 2007 is presented in Fig. 8.

In order to check the benefit of having calibrated our retrieval algorithm independently for both F13 and F17 instruments, we compared the estimated LSTs obtained from each sensor on the overlap period of summer 2008. The spatial distribution of the biases and RMSEs obtained are plotted in Fig. 9.

The mean bias and RMSE are respectively 0.15 K and 1.2 K, which appear quite satisfactory. As a comparison, these metrics are equal to 1 K and 3 K if constant parameters such as proposed by Mialon et al. (2007) are used.

For evaluation purposes, the SSM/I derived LST product was compared with MODIS data filtered following the same methodology explained in Section 3.3 to eliminate outliers.

Fig. 10 shows the scatterplot between MODIS and SSM/I-derived temperatures (Fig. 9 left) and the distribution of the RMSEs (Fig. 9 right) calculated for summer 2008. The average value of the RMSEs (2.4 K) is slightly larger than in 2007 (2.15 K) but still quite acceptable. The regression line plotted in Fig. 10 shows a slight overestimation (underestimation) for low (high) temperatures (slope of 0.92). This trend could be the result of both remaining clouds in MODIS LST despite the rigorous filtering process and the over-smoothing of the SSM/I LST diurnal cycle already mentioned. In order to better assess the performances of the retrieval methodology and the accuracy of our product, the evaluation against MODIS LST data was extended temporally to snow free periods ranging from 2004 to 2010. The time period was chosen in order to benefit from both Terra and Aqua instruments and to cover a large part of the interannual variability. The comparison at circumpolar scale (not shown here graphically) shows satisfactory results with an average RMSE equal to 2.19 K (ranging from 2.08 to 2.40 K, depending on the year) and a low average bias of 0.33 ± 0.10 K over the 7 years analyzed. Similar spatial patterns also appear, demonstrating the robustness of our algorithm and the overall good accuracy of the LST continuous time series produced.

To better analyze the limits of our methodology and the errors obtained, the spatial variations of the RMSEs have been studied in relation to surface characteristics, in particular land cover, using the ESA CCI land cover map introduced in Section 2.5. The original resolution of 300 m was used to calculate the land cover fractions at the EASE grid scale. The dominant land cover class in the aggregated pixel was kept to discriminate the pixels and the map showing the resulting six main classes present in the circumpolar northern latitudes: bare soil, tundra (merge of sparse vegetation and lichen and mosses classes), croplands, grasslands, needleleaf and broadleaf forests, are shown in Fig. 11.

Table 3 shows biases, RMSEs and correlation between SSM/I-derived temperatures against MODIS LST for the six main land cover classes. The columns are sorted in descending RMSE order, ranging from 3.3 to 2.1 K. As highlighted by Njoku and Li (1999), the error is lower for forests or dense vegetation cover compared to the classes with sparse or no vegetation. The error increases on bare soil and on sparse vegetation covers for which the sensitivity of the surface emissivity to soil moisture variations is higher, which means that the assumption of a constant relationship linking polarized emissivities could be less valid. The biases stay very low however, between 0.7 and 0.4 K for all classes.

Table 3
Bias, RMSE and correlation of SSM/I-derived LST against MODIS LST for the snow-free period of 2008, for each of vegetation considered (see Fig. 10).

	Bare soil	Grassland	Cropland	Tundra	Needleleaf	Broadleaf
Bias (K)	0.66	0.59	0.46	0.41	0.43	0.62
RMSE (K)	3.32	3.01	2.49	2.32	2.16	2.06
Correlation	0.97	0.96	0.96	0.96	0.96	0.95

5. Conclusions

This study presents the methodology that was developed to estimate LST continuous time series from the SSM/I passive microwave brightness temperatures. The algorithm based on the approach proposed by Royer and Poirier (2010), was refined to take advantage of the concurrent MODIS thermal infrared data. These auxiliary data, requiring cloud-free conditions but considered reliable, were used to calibrate the radiative transfer model inversion and separate emissivity and temperature at pixel scale. The calibration was performed independently for F13 and F17 sensors during the training time overlap period of summer 2007. Consequently, this methodology is not affected by the inter-calibration problems between both SSM/I sensors. The synchronization between the MODIS and SSM/I data and the use of skin surface temperature reanalysis data allowed us to produce LST time series at an hourly time step and 25 km scale for the 10-year period (2000–2011) with two snow-free seasons of overlap between the F13 and F17 sensors (2007–2008). The LST time series were produced on land and ice-free pixels over the circumpolar Northern Hemisphere (latitudes larger than 45° N) and during snow-free periods.

This new LST product was first evaluated at pixel scale for five experimental sites in the Arctic. The results show a very good agreement with MODIS LST data on daily mean time series, with a mean bias less than 0.4 K and a RMSE of about 2 K. The comparison also shows the advantages of the microwave measurements, which are not sensitive to clouds compared to thermal infrared products, in spite of the coarser resolution of SSM/I data compared to MODIS. The results also highlight the deficiencies of cloud detection in the MODIS product.

The SSM/I product was also evaluated at larger scale over all northern latitudes for a time period of seven years (2004–2010) against MODIS LST data. The comparison shows good reliability, with correlation, biases and RMSE equal to 0.96, 0.3 K and 2.2 K, respectively. The error analysis showed the impact of land cover on the algorithm estimates. Indeed, it was shown that the best results are obtained for forested areas and the worse estimates for bare surfaces. This result was expected since larger variability of the surface emissivity and its spectral properties is expected for bare soil pixels, leading to larger errors in the LST retrieval from microwave measurements. Nevertheless,

the produced LST time series are valuable data for LST and land surface model monitoring in the Arctic. The daily LST can be downloaded from the PANGAEA website (http://doi.pangaea.de/10.1594/PANGAEA.833409) and data at hourly time steps will be soon available on the EU PAGE21 project website (http://www.page21.eu/). Future research will include the extension of the time series to the former SSM/I instruments to cover the whole period (1978–2013).

Acknowledgments

This work was supported by the PAGE21 project (grant agreement number 282700, funded by the EC seventh Framework Programme theme FP7-ENV-2011) and NSERC-Canada projects. The authors are grateful to the site PIs for providing the in-situ data: Julia Boike and Moritz Langer for the Samoylov site, Annika Kristoffersson for Abisko, Elyn Humphrey and Peter Lafleur for Daring Lake, Syndonia Bret-Harte for Cherskii, Douglas Kane and Larry Hinzman for North Slope and also to NASA, ESA, ECMWF and NSIDC for making their datasets available for this work. We also acknowledge Alexandre Roy who provided the relationships for the atmospheric corrections, Julia Boike and Michel Fily for helpful discussions and Annett Bartsch and Elin Hogström for initiating scientific interactions within the PAGE21 project.

Abisko temperatures were available from the Abisko Research Station (automatic weather station). Web site: http://www.polar.se/abisko.

North Slope temperatures were provided by the North Slope Hydrology Research project, UAF, Water and Environmental Research Center (http://ine.uaf.edu/werc/projects/).

Cherskii temperatures were provided by the Institute of Arctic Biology, UAF, based upon work supported by the National Science Foundation under grant # 1107892. The data are available on the website:http://aon.iab.uaf.edu/data_access.

Daring Lake measurements were provided with funding support from the Canadian Foundation for Climate and Atmospheric Sciences, Natural Sciences and Engineering Research Council of Canada, International Polar Year — Government of Canada, Polar Continental Shelf Project, Canada Foundation for Innovation and Ontario Innovation Trust and assistance from staff at the Daring Lake Tundra Ecosystem Research Station.

The following datasets were downloaded from:

- The National Snow and Ice Data Center:
  SSM/I (ftp://sidads.colorado.edu/pub/DATASETS/nsidc0032_ease_grid_tbs/),
  EASE-Grid Land Cover Data Resampled from Boston University Version of Global 1 km Land Cover from MODIS 2001, Version 4 (https://nsidc.org/data/ease/ancillary.html#bumodis).
- The U.S. Geological Survey (http://e4ftl01.cr.usgs.gov) for the MODIS datasets.
- ECMWF (http://apps.ecmwf.int/datasets/data/interim_land/) for the ERA-Interim and (http://data-portal.ecmwf.int/data/d/era40_daily/) for the ERA-40 datasets.
- ESA (http://maps.elie.ucl.ac.be/CCI/viewer_new/) for the CCI land cover map.
- NCEP Reanalysis data provided by the NOAA/OAR/ESRL PSD, Boulder, Colorado, USA, from their Web site at http://www.cdc.noaa.gov/.

References

Ackerman, S. A., Holz, R. E., Frey, R., Eloranta, E. W., Maddux, B. C., & McGill, M. (2008). Cloud detection with MODIS. Part II: Validation. *Journal of Atmospheric & Oceanic Technology*, *25*(7).

Aires, F., Prigent, C., & Rossow, W. B. (2004). Temporal interpolation of global surface skin temperature diurnal cycle over land under clear and cloudy conditions. *Journal of Geophysical Research*, *109*, D04313. http://dx.doi.org/10.1029/2003JD003527.

Aires, F., Prigent, C., Rossow, W. B., & Rothstein, M. (2001). A new neural network approach including first-guess for retrieval of atmospheric water vapor, cloud liquid water path, surface temperature and emissivities over land from satellite microwave observations. *Journal of Geophysical Research*, *106*, 14887–14907.

AMAP (2011). *SWIPA (snow, water, ice, and permafrost in the Arctic) executive summary*. Oslo, Norway: Arctic Monitoring and Assessment Program (15 pp.).

Anisimov, O. A., Lobanov, V. A., Reneva, S. A., Shiklomanov, N. I., Zhang, T., & Nelson, F. E. (2007). Uncertainties in gridded air temperature fields and effects on predictive active layout modeling. *Journal of Geophysical Research*, *112*, F02S14. http://dx.doi.org/10.1029/2006JF000593.

Armstrong, R. L., & Brodzik, M. J. (1995). An Earth-gridded SSM/I data set for cryospheric studies and global change monitoring. *Advances in Space Research*, *16*(10), 155–163.

Armstrong, R., Knowles, K., Brodzik, M., & Hardman, M. (1994). *DMSP SSM/I Pathfinder daily EASE-Grid brightness temperatures*. Boulder, CO, USA: National Snow and Ice Data Center, digital media and CD-ROM (updated 2008).

Becker, F., & Li, Z. L. (1995). Surface temperature and emissivity at various scales: Definition, measurement and related problems. *Remote Sensing Reviews*, *12*, 225–253.

Betts, A. K., Ball, J. H., & Viterbo, P. (2003). Evaluation of the ERA-40 surface water budget and surface air temperature for the Mackenzie River basin. *Journal of Hydrometeorology*, *4*, 1194–1211.

Boike, J., Kattenstroth, B., Abramova, K., Bornemann, N., Chetverova, A., Fedorova, I., et al. (2013). Baseline characteristics of climate, permafrost and land cover from a new permafrost observatory in the Lena River Delta, Siberia (1998–2011). *Biogeosciences*, *10*, 2105–2128. http://dx.doi.org/10.5194/bg-10-2105-2013.

Bontemps, S., Defourny, P., Radoux, J., Van Bogaert, E., Lamarche, C., Achard, F., et al. (2013). Consistent global land cover maps for climate modelling communities: current achievements of the ESA's land cover CCI. *Proceedings of the ESA Living Planet Symposium, Edinburgh, 9–13 September*.

Bromwich, D. H., Fogt, R. L., Hodges, K. I., & Walsh, J. E. (2007). A tropospheric assessment of the ERA-40, NCEP, and JRA-25 global reanalyses in the Polar Regions. *Journal of Geophysical Research*, *112*, D10111. http://dx.doi.org/10.1029/2006JD007859.

Bunn, A. G., Goetz, S. J., Kimball, J. S., & Zhang, K. (2007). Northern high-latitude ecosystems respond to climate change. *Eos, Transactions American Geophysical Union*, *88*(34), 333–335.

Catherinot, J., Prigent, C., Maurer, R., Papa, F., Jiménez, C., Aires, F., et al. (2011). Evaluation of "all weather" microwave-derived land surface temperatures with in situ CEOP measurements. *Journal of Geophysical Research*, *116*, D23105. http://dx.doi.org/10.1029/2011JD016439.

Cavalieri, D. J., Parkinson, C. L., DiGirolamo, N., & Ivanoff, A. (2012). Intersensor calibration between F13 SSMI and F17 SSMIS for global sea ice data records. *Geoscience and Remote Sensing Letters, IEEE*, *9*(2), 233–236. http://dx.doi.org/10.1109/LGRS.2011.2166754.

Dee, D. P., Uppala, S. M., Simmons, A. J., et al. (2011). The ERA-Interim reanalysis: Configuration and performance of the data assimilation system. *Quarterly Journal of the Royal Meteorological Society*, *137*, 553–597.

Derksen, C., Silis, A., Sturm, M., Holmgren, J., Liston, G. E., Huntington, H., et al. (2009). Northwest Territories and Nunavut snow characteristics from a subarctic traverse: Implications for passive microwave remote sensing. *Journal of Hydrometeorology*, *10*(2), 448–463.

Eastman, R., & Warren, S. G. (2010). Interannual variations of Arctic cloud types in relation to sea ice. *Journal of Climate*, *23*, 4216–4232. http://dx.doi.org/10.1175/2010JCLI3492.1.

Euskirchen, E. S., McGuire, A. D., Kicklighter, D. W., Zhuang, Q., Clein, J. S., Dargaville, R. J., et al. (2006). Importance of recent shifts in soil thermal dynamics on growing season length, productivity, and carbon sequestration in terrestrial high-latitude ecosystems. *Global Change Biology*, *12*(4), 731–750.

Fily, M., Royer, A., Goïta, K., & Prigent, C. (2003). A simple retrieval method for land surface temperature and fraction of water surface determination from satellite microwave brightness temperatures in sub-Arctic areas. *Remote Sensing of Environment*, *85*, 328–338.

Goïta, K., & Royer, A. (2002). Combination of passive microwave and thermal infrared for the retrieval and analysis of microwave emissivities and temperature. *IEEE International Geoscience and Remote Sensing Symposium, 2002. IGARSS '02. Vol. 4.* (pp. 2401–2403). http://dx.doi.org/10.1109/IGARSS.2002.1026557 (24–28 June 2002).

Goulden, M. L., et al. (1998). Sensitivity of boreal forest carbon balance to soil thaw. *Science*, *279*, 214–217.

Gutman, G., Tarpley, D., Ignatov, A., & Olson, S. (1998). Global AVHRR products for land climate studies. *Advances in Space Research*, *22*(11), 1591–1594.

Hachem, S., Allard, M., & Duguay, C. (2009). Using the MODIS land surface temperature product for mapping permafrost: An application to northern Québec and Labrador, Canada. *Permafrost and Periglac Process*, *20*, 407–416. http://dx.doi.org/10.1002/ppp.672.

Hachem, S., Duguay, C. R., & Allard, M. (2012). Comparison of MODIS-derived land surface temperatures with ground surface and air temperature measurements in continuous permafrost terrain. *The Cryosphere*, *6*(1), 51–69.

Hartmann, D. L., Klein Tank, A. M. G., Rusticucci, M., Alexander, L. V., Brönnimann, S., Charabi, Y., et al. (2013). Observations: Atmosphere and surface. *Climate Change 2013: The physical science basis. Contribution of working group I to the Fifth Assessment Report of the Intergovernmental Panel on Climate Change*. Cambridge, United Kingdom and New York, NY, USA: Cambridge University Press.

Hashimoto, H., Dungan, J. L., White, M. A., Yang, F., Michaelis, A. R., Running, S. W., et al. (2008). Satellite-based estimation of surface vapor pressure deficits using MODIS land surface temperature data. *Remote Sensing of Environment*, *112*(1), 142–155. http://dx.doi.org/10.1016/j.rse.2007.04.016.

Hinkel, K. M., & Nelson, F. E. (2003). Spatial and temporal patterns of active layer thickness at Circumpolar Active Layer Monitoring (CALM) sites in northern Alaska, 1995–2000. *Journal of Geophysical Research: Atmospheres (1984–2012)*, *108*(D2).

Holmes, T. R., Crow, W. T., Tugrul Yilmaz, M., Jackson, T. J., & Basara, J. B. (2013). Enhancing model-based land surface temperature estimates using multiplatform microwave observations. *Journal of Geophysical Research*, *118*(2), 577–591.

Holmes, T. R., De Jeu, R. A. M., Owe, M., & Dolman, A. J. (2009). Land surface temperature from Ka band (37 GHz) passive microwave observations. *Journal of Geophysical Research*, *114*, D04113. http://dx.doi.org/10.1029/2008JD010257.

Jones, L. A., Ferguson, C. R., Kimball, J. S., Zhang, K., Chan, S. T. K., McDonnald, K. C., et al. (2010). Satellite microwave remote sensing of daily land surface air temperature minima and maxima from AMSR-E. *IEEE Journal of Selection Topics in Applied Earth Observations Remote Sensing*, *3*, 111–123.

Jones, L. A., Kimball, J. S., McDonald, K. C., Chan, S. T. K., Njoku, E. G., & Oechel, W. C. (2007). Satellite microwave remote sensing of boreal and arctic soil temperatures from AMSR-E. *IEEE Transactions on Geoscience and Remote Sensing*, *45*(7), 2004–2018.

Kalma, J. D., McVicar, T. R., & McCabe, M. F. (2008). Estimating land surface evaporation: A review of methods using remotely sensed surface temperature data. *Surveys in Geophysics*, *29*, 421–469. http://dx.doi.org/10.1007/s10712-008-9037-z.

Kerr, Y. H., & Njoku, E. G. (1990). A semi empirical model for interpreting microwave emission from semiarid land surfaces as seen from space. *IEEE Transactions on Geoscience and Remote Sensing*, *28*, 384–393.

Kim, Y., Kimball, J. S., Zhang, K., & McDonald, K. C. (2012). Satellite detection of increasing Northern Hemisphere non-frozen seasons from 1979 to 2008: Implications for regional vegetation growth. *Remote Sensing of Environment*, *121*, 472–487. http://dx.doi.org/10.1016/j.rse.2012.02.014.

Kimball, J. S., McDonald, K. C., & Zhao, M. (2006). Spring thaw and its effect on terrestrial vegetation productivity in the western Arctic observed from satellite microwave and optical remote sensing. *Earth Interactions*, *10*(21), 1–22.

Knowles, K. (2004). *EASE-Grid land cover data resampled from Boston University version of global 1 km land cover from MODIS 2001, version 4.* Boulder, Colorado USA: National Snow and Ice Data Center. Digital Media.

Kuzmina, S. I., Johannessen, O. M., Bengtsson, L., Aniskina, O. G., & Bobylev, L. P. (2008). High northern latitude surface air temperature: comparison of existing data and creation of a new gridded data set 1900–2000. *Tellus*, *60A*, 289–304.

Lanckman, J. P., Elger, K., Karlsson, Æ. K., Johannsson, H., & Lantuit, H. (2013). The GTN-P data management system: A central database for permafrost monitoring parameters of the Global Terrestrial Network for Permafrost (GTN-P) and beyond. *EGU General Assembly Conference Abstracts. Vol. 15.* (pp. 7808).

Langer, M., Westermann, S., & Boike, J. (2010). Spatial and temporal variations of summer surface temperatures of wet polygonal tundra in Siberia — Implications for MODIS LST based permafrost monitoring. *Remote Sensing of Environment*, *114*(9), 2059–2069.

Langer, M., Westermann, S., Heikenfeld, M., Dorn, W., & Boike, J. (2013). Satellite-based modeling of permafrost temperatures in a tundra lowland landscape. *Remote Sensing of Environment*, *135*, 12–24.

Liebe, H. (1989). MPM: An atmospheric millimeter-wave propagation model. *International Journal of Infrared and Millimeter Waves*, *10*(6), 631–650.

Lindsay, R., Wensnahan, M., Schweiger, A., & Zhang, J. (2014). Evaluation of seven different atmospheric reanalysis products in the Arctic. *Journal of Climate*, *27*, 2588–2606. http://dx.doi.org/10.1175/JCLI-D-13-00014.1.

Luo, Y., Berbery, E. H., Mitchell, K. E., & Betts, A. K. (2007). Relationships between land surface and near-surface atmospheric variables in the NCEP North American regional reanalysis. *Journal of Hydrometeorology*, *8*, 1184–1204.

Ma, L., Zhang, T., Li, Q., Frauenfeld, O. W., & Qin, D. (2008). Evaluation of ERA-40, NCEP-1, and NCEP-2 reanalysis air temperatures with ground-based measurements in China. *Journal of Geophysical Research*, *113*, D15115. http://dx.doi.org/10.1029/2007JD009549.

Matzner, E., & Borken, W. (2008). Do freeze–thaw events enhance C and N losses from soils of different ecosystems? A review. *European Journal of Soil Science*. http://dx.doi.org/10.1111/j.1365-2389.2007.00992.x.

McGuire, A. D., Chapin, F. S., III, Wirth, C., Apps, M. J., Bhatti, J. S., Callaghan, T., et al. (2007). Responses of high latitude ecosystems to global change: Potential consequences for the climate system. In J. G. Canadell, D. E. Pataki, & L. F. Pitelka (Eds.), *Terrestrial ecosystems in a changing world. IGBP Series*. (pp. 297–310). New York, New York, USA: Springer (Vol. Chapter 24).

Mesinger, F., Dimego, G., Kalnay, E., Mitchell, K., Shafran, P. C., Ebisuzaki, W., et al. (2006). North American regional reanalysis. *Bulletin of the American Meteorological Society*, *87*(3), 343–360.

Mialon, A., Royer, A., Fily, M., & Picard, G. (2007). Daily microwave derived surface temperature over Canada/Alaska. *Journal of Applied Meteorology and Climatology*, *46*(5), 591–604.

Nemani, R. R., Keeling, C. D., Hashimoto, H., Jolly, W. M., Piper, S. C., Tucker, C. J., et al. (2003). Climate-driven increases in global terrestrial net primary production from 1982 to 1999. *Science*, *300*(5625), 1560–1562.

Njoku, E. G., & Li, L. (1999). Retrieval of land surface parameters using passive microwave measurements at 6–18 GHz. *IEEE Transactions on Geoscience and Remote Sensing*, *37*(1), 79–93.

Oechel, W. C., Hastings, S. J., Vourlitis, G., Jenkins, M., Riechers, G., & Grulke, N. (1993). Recent change of Arctic tundra ecosystems from a net carbon dioxide sink to a source. *Nature*, *361*, 520–523. http://dx.doi.org/10.1038/361520a0.

Oelke, C., Zhang, T., & Serreze, M. C. (2004). Modelling evidence for recent warming of the Arctic soil thermal regime. *Geophysical Research Letters*, *31*(7). http://dx.doi.org/10.1029/2003GL019300.

Oelke, C., Zhang, T., Serreze, M. C., & Armstrong, R. L. (2003). Regional-scale modeling of soil freeze/thaw over the Arctic drainage basin. *Journal of Geophysical Research*, *108*(D10), 4314. http://dx.doi.org/10.1029/2002JD002722.

Østby, T., Schuler, T., & Westermann, S. (2014). Severe cloud contamination of MODIS land surface temperatures over an Arctic ice cap, Svalbard. *Remote Sensing of Environment*0034-4257, *142*, 95–102.

Overland, J., Key, J., Hanna, E., Hanssen-Bauer, I., Kim, B. -M., Kim, S. -J., et al. (2014). [The Arctic] The lower atmosphere: air temperature, clouds and surface radiation [in "State of the Climate in 2013"]. *Bulletin of the American Meteorological Society*, *95*(7), S115–S117.

Pampaloni, P., & Paloscia, S. (1985). Experimental relationships between microwave emission and vegetation features. *International Journal of Remote Sensing*, *6*(2), 315–323.

Parinussa, R. M., de Jeu, R. A., Holmes, T. R., & Walker, J. P. (2008). Comparison of microwave and infrared land surface temperature products over the NAFE'06 research sites. *IEEE Geoscience and Remote Sensing Letters*, *5*(4), 783–787.

Piao, S., Ciais, P., Friedlingstein, P., Peylin, P., Reichstein, M., Luyssaert, S., et al. (2008). Net carbon dioxide losses of northern ecosystems in response to autumn warming. *Nature*, *451*(7174), 49–52.

Pulliainen, J., Grandell, T., & Hallikainen, J. (1999). Hut snow emission model and its applicability to snow water equivalent retrieval. *IEEE Transactions on Geoscience and Remote Sensing*, *37*, 1378–1390.

Roy, A. (2014). *Modélisation de l'émission micro-onde hivernale en forêt boréale canadienne.* (Ph.D. thesis) Université de Sherbrooke (222 pp.).

Royer, A., & Poirier, S. (2010). Surface temperature spatial and temporal variations in North America from homogenized satellite SMMR-SSM/I microwave measurements and reanalysis for 1979–2008. *Journal of Geophysical Research*, *115*, D08110. http://dx.doi.org/10.1029/2009JD012760.

Running, S. W., & Kimball, J. S. (2005). Satellite-based analysis of ecological controls for land-surface evaporation resistance. *Encyclopedia of hydrological sciences*. Hoboken, NJ: Wiley.

Sims, D. A., Rahman, A. F., Cordova, V. D., El-Masri, B. Z., Baldocchi, D. D., Bolstad, P. V., et al. (2008). A new model of gross primary productivity for North American ecosystems based solely on the enhanced vegetation index and land surface temperature from MODIS. *Remote Sensing of Environment*, *112*(4), 1633–1646.

Soliman, A., Duguay, C., Saunders, W., & Hachem, S. (2012). Pan-Arctic land surface temperature from MODIS and AATSR: Product development and intercomparison. *Remote Sensing*, *4*(12), 3833–3856.

Taylor, K. E. (2001). Summarizing multiple aspects of model performance in single diagram. *Journal of Geophysical Research*, *106*(D7), 7183–7192.

Trigo, I. F., Monteiro, I. T., Olesen, F., & Kabsch, E. (2008). An assessment of remotely sensed land surface temperature. *Journal of Geophysical Research*, *113*, 1708–1719.

Tsuang, B. -J., Chou, M. -D., Zhang, Y. -C., & Roesch, A. (2008). Evaluation of land–ocean skin temperatures of the ISCCP satellite retrievals and the NCEP and ERA reanalyses. *Journal of Climate*, *21*, 308–330. http://dx.doi.org/10.1175/2007JCLI1502.1.

Uppala, S. M., KÅllberg, P. W., Simmons, A. J., Andrae, U., Bechtold, V. D. C., Fiorino, M., et al. (2005). The ERA-40 re-analysis. *Quarterly Journal of the Royal Meteorological Society*, *131*(612), 2961–3012.

Wan, Z. (2008). New refinements and validation of the MODIS land-surface temperature/emissivity products. *Remote Sensing of Environment*, *112*(1), 59–74.

Westermann, S., Langer, M., & Boike, J. (2011). Spatial and temporal variations of summer surface temperatures of high-Arctic tundra on Svalbard—Implications for MODIS LST based permafrost monitoring. *Remote Sensing of Environment*, *115*(3), 908–922.

Westermann, S., Langer, M., & Boike, J. (2012). Systematic bias of average winter-time land surface temperatures inferred from MODIS at a site on Svalbard, Norway. *Remote Sensing of Environment*, *118*, 162–167.

Xiong, X., Wu, A., & Cao, C. (2008). On-orbit calibration and inter-comparison of Terra and Aqua MODIS surface temperature spectral bands. *International Journal of Remote Sensing*, *29*(17), 5347–5359.

Zhang, Yu., Chen, W., Smith, S. L., Riseborough, D. W., & Cihlar, J. (2005). Soil temperature in Canada during the twentieth century: Complex responses to atmospheric climate change. *Journal of Geophysical Research*, *110*, D03112. http://dx.doi.org/10.1029/2004JD004910.

Zou, H., Zhu, J., Zhou, L., Li, P., & Ma, S. (2014). Validation and application of reanalysis temperature data over the Tibetan Plateau. *Journal of the Meteorological Society*, *28*(1), 139–149. http://dx.doi.org/10.1007/s13351-014-3027-5.